

# Singlet Dark Matter in Type II Two Higgs Doublet Model

Yi Cai<sup>a\*</sup> and Tong Li<sup>b†</sup>

<sup>a</sup> *ARC Centre of Excellence for Particle Physics at the Terascale,  
School of Physics, University of Melbourne, Melbourne, Victoria 3010, Australia*

<sup>b</sup> *ARC Centre of Excellence for Particle Physics at the Terascale,  
School of Physics, Monash University, Melbourne, Victoria 3800, Australia*

## Abstract

Inspired by the dark matter searches in the low mass region, we study the Type II two Higgs doublet model with a light gauge singlet WIMP stabilized by a  $Z_2$  symmetry. The real singlet is required to only couple to the non-Standard Model Higgs. We investigate singlet candidates with different spins as well as isospin violating effect. The parameter space favored by LHC data in two Higgs doublet model and hadronic uncertainties in WIMP-nucleon elastic scattering are also taken into account. We find only the scalar singlet in the isospin conserving case leads to a major overlap with the region of interests of most direct detection experiments.

---

\*Electronic address: [yi.cai@unimelb.edu.au](mailto:yi.cai@unimelb.edu.au)

†Electronic address: [tong.li@monash.edu](mailto:tong.li@monash.edu)

## I. INTRODUCTION

The existence of some mysterious component of the Universe, namely the dark matter (DM), has been solidified by multiple astrophysical and cosmological observations. The weakly interacting massive particle (WIMP) is one popular candidate of DM. Recently various underground direct detection experiments such as DAMA [1], CoGeNT [2], CRESST [3] and CDMS [4] have shown some DM-like events in the low mass region. Although there is still no conclusive statement for the existence of WIMP based on these events, it is worth paying special attention to the light WIMP considering undergoing searches in low mass region.

Since there is no viable WIMP candidates in the Standard Model (SM), extensions of this highly successful theory is necessary. One simple extension of the SM is to add a real SM gauge singlet with a mass of the electroweak scale or less [5–7]. An unbroken  $Z_2$  parity, under which only the singlet is odd, stabilizes this particle (called  $D$  here).

At the renormalizable level the singlet only couples to the SM Higgs doublet. The coupling has to be carefully adjusted to reproduce the required relic density of  $D$ , while satisfying the constraints from the indirect and direct searches [8–10]. It is, however, a hard task to accomplish within the SM+ $D$  framework, taking into account the results from the direct detection of DM and the search for invisible decay mode of SM Higgs at the LHC. For recent discussions, see Ref. [11] and references therein. In order to achieve a consistent scenario with singlet dark matter, it is desirable to consider an extension of the SM, such as the Two Higgs doublet model (THDM) that we discuss here [10, 12].

In this paper we study the THDM+ $D$  framework, with singlet mass  $\lesssim 20$  GeV, in light of the implications of the LHC Higgs search results for the Type II THDM. To accommodate the SM Higgs search data, the coupling between the singlet and the SM-like Higgs is forbidden by hand and DM  $D$  can only be produced in pairs via the non-SM Higgs boson. In particular the isospin-violating effect introduced to reconcile the experiments above and XENON100 is discussed [13], in terms of the allowed parameter region in Type II THDM. We investigate three candidates of real singlet field, namely scalar, Majorana fermion and vector.

The paper is organized as follows. In Sec. II we describe the properties of THDM+ $D$  framework, where we also discuss the constraints on Type II THDM from the LHC Higgs search. The results of  $D$ -Higgs scattering interaction are presented in Sec. III. In this section we also display the  $D$ -nucleon elastic cross sections. We summarize our conclusions in Sec. IV.

## II. SINGLET DARK MATTER IN TYPE II THDM

### A. Model and Experimental Constraints

The interactions between the scalar  $S$ , Majorana fermion  $\chi$ , vector  $V_\mu$  singlet and Higgs sector in the Type II THDM are

$$\mathcal{L}_S = -\frac{1}{2}S^2(\lambda_{S1}H_1^\dagger H_1 + \lambda_{S2}H_2^\dagger H_2) - \frac{m_{S0}^2}{2}S^2 - \frac{\lambda'_S}{4!}S^4, \quad (1)$$

$$\mathcal{L}_\chi = -\frac{1}{2\Lambda}\bar{\chi}^c\chi(\lambda_{\chi1}H_1^\dagger H_1 + \lambda_{\chi2}H_2^\dagger H_2) - \frac{m_\chi}{2}\bar{\chi}^c\chi + h.c., \quad (2)$$

$$\mathcal{L}_V = \frac{1}{2}V_\mu V^\mu(\lambda_{V1}H_1^\dagger H_1 + \lambda_{V2}H_2^\dagger H_2) + \frac{m_V^2}{2}V_\mu V^\mu - \frac{\lambda'_V}{4!}(V_\mu V^\mu)^2 - \frac{1}{4}V^{\mu\nu}V_{\mu\nu}, \quad (3)$$

where  $\Lambda$  is a dimensional scale for fermionic singlet. Note that a discrete  $Z'_2$  symmetry, under which only  $H_2$  is odd, is introduced here to forbid other Higgs interactions. The two Higgs doublets are decomposed as

$$H_i = \begin{pmatrix} h_i^+ \\ (v_i + h_i + iP_i)/\sqrt{2} \end{pmatrix} \quad i = 1, 2, \quad \begin{pmatrix} h_1^+ \\ h_2^+ \end{pmatrix} = \begin{pmatrix} \cos\beta & -\sin\beta \\ \sin\beta & \cos\beta \end{pmatrix} \begin{pmatrix} G^+ \\ H^+ \end{pmatrix}, \quad (4)$$

$$\begin{pmatrix} P_1 \\ P_2 \end{pmatrix} = \begin{pmatrix} \cos\beta & -\sin\beta \\ \sin\beta & \cos\beta \end{pmatrix} \begin{pmatrix} G^0 \\ A^0 \end{pmatrix}, \quad \begin{pmatrix} h_1 \\ h_2 \end{pmatrix} = \begin{pmatrix} \cos\alpha & -\sin\alpha \\ \sin\alpha & \cos\alpha \end{pmatrix} \begin{pmatrix} H^0 \\ h^0 \end{pmatrix}, \quad (5)$$

with  $\tan\beta = v_2/v_1$ ,  $v_0^2 = v_1^2 + v_2^2 \approx (246 \text{ GeV})^2$  and  $\alpha$  being the mixing angle between two neutral CP-even Higgses. After the electroweak symmetry breaking, one gets the following DM interactions with the neutral CP-even Higgses

$$\mathcal{L}_{SSH} = -(-\lambda_{S1}\sin\alpha\cos\beta + \lambda_{S2}\cos\alpha\sin\beta)v_0S^2h^0/2 \equiv -\lambda_{Sh}v_0S^2h^0/2, \quad (6)$$

$$\mathcal{L}_{SSH} = -(\lambda_{S1}\cos\alpha\cos\beta + \lambda_{S2}\sin\alpha\sin\beta)v_0S^2H^0/2 \equiv -\lambda_{SH}v_0S^2H^0/2, \quad (7)$$

for scalar candidate  $S$ ,

$$\mathcal{L}_{FFh} = -(-\lambda_{\chi1}\sin\alpha\cos\beta + \lambda_{\chi2}\cos\alpha\sin\beta)v_0\bar{\chi}^c\chi h^0/\Lambda \equiv \lambda_{Fh}F^2h^0/2, \quad (8)$$

$$\mathcal{L}_{FFH} = -(\lambda_{\chi1}\cos\alpha\cos\beta + \lambda_{\chi2}\sin\alpha\sin\beta)v_0\bar{\chi}^c\chi H^0/\Lambda \equiv -\lambda_{FH}F^2H^0/2, \quad (9)$$

for fermion candidate  $F = \chi + \chi^c$  and

$$\mathcal{L}_{VVh} = (-\lambda_{V1}\sin\alpha\cos\beta + \lambda_{V2}\cos\alpha\sin\beta)v_0V^2h^0/2 \equiv \lambda_{Vh}v_0V^2h^0/2, \quad (10)$$

$$\mathcal{L}_{VVH} = (\lambda_{V1}\cos\alpha\cos\beta + \lambda_{V2}\sin\alpha\sin\beta)v_0V^2H^0/2 \equiv \lambda_{VH}v_0V^2H^0/2, \quad (11)$$

for vector candidate  $V$  respectively. The size of the couplings  $\lambda_{D\mathcal{H}}$  ( $D = S, F, V; \mathcal{H} = h^0, H^0$ ) controls the signal strength of the DM detection and is determined by the constraints from DM relic density measurement and the implication of SM Higgs searches for THDM at LHC.

In the Type II THDM, the interactions between two CP-even Higgses and massive gauge bosons follow the same behavior as in the Minimal Supersymmetric Standard Model (MSSM):

$$\mathcal{L}_{\mathcal{H}WW/ZZ} = \left( \frac{2m_W^2}{v_0} WW + \frac{m_Z^2}{v_0} ZZ \right) (h^0 \sin(\beta - \alpha) + H^0 \cos(\beta - \alpha)), \quad (12)$$

where SM-like Higgs is the one which couples to the gauge bosons more strongly. Current studies of the LHC data and the Type II THDM imply the existence of two scenarios [14]

$$\begin{aligned} I : \quad & \sin(\beta - \alpha) \approx \pm 1, h^0 \text{ SM-like}, \\ & 100 < M_{H^0} < 750 \text{ GeV}, 300 < M_{H^\pm} < 800 \text{ GeV}, M_A < 800 \text{ GeV}; \end{aligned} \quad (13)$$

$$\begin{aligned} II : \quad & \sin(\beta - \alpha) \approx 0, H^0 \text{ SM-like}, \\ & 70 < M_{h^0} < 126 \text{ GeV}, M_A \simeq M_{H^\pm} > 300 \text{ GeV}, \end{aligned} \quad (14)$$

with  $0.5 < \tan \beta < 4$  in both cases. Unlike the MSSM, in Type II THDM, the masses of  $H^0, A^0, H^\pm$  are largely uncorrelated. In order to simplify the non-SM Higgs decay modes for concreteness, we take the degenerate case, namely  $M_{H^0} \approx M_{A^0} \approx M_{H^\pm}$ , in scenario I.

## B. Singlet DM Annihilation and Singlet-Nucleon Scattering Interaction

As mentioned in the introduction, in order to accommodate a small SM Higgs invisible decay branching ratio, we set vanishing couplings  $\lambda_{Dh^0}(\lambda_{DH^0}) = 0$  in scenario I (II). Thus the DM singlets can only be produced in pairs from non-SM Higgs decay. The partial widths of the Higgs boson  $\mathcal{H}$  decay into DM singlet are given by [15]

$$\Gamma_S = \frac{\lambda_{S\mathcal{H}}^2 v_0^2}{32\pi m_{\mathcal{H}}} \sqrt{1 - \frac{4m_S^2}{m_{\mathcal{H}}^2}}, \quad (15)$$

$$\Gamma_F = \frac{\lambda_{F\mathcal{H}}^2 m_{\mathcal{H}}}{16\pi} \left( 1 - \frac{4m_F^2}{m_{\mathcal{H}}^2} \right)^{3/2}, \quad (16)$$

$$\Gamma_V = \frac{\lambda_{V\mathcal{H}}^2 v_0^2 m_{\mathcal{H}}^3}{128\pi m_V^4} \left( 1 - \frac{4m_V^2}{m_{\mathcal{H}}^2} + \frac{12m_V^4}{m_{\mathcal{H}}^4} \right) \sqrt{1 - \frac{4m_V^2}{m_{\mathcal{H}}^2}}. \quad (17)$$

The  $\mathcal{H}$ -mediated annihilation cross sections of DM singlets are thus

$$\sigma_{ann} v_{rel}(S) = \frac{2\lambda_{S\mathcal{H}}^2 v_0^2}{(4m_S^2 - m_{\mathcal{H}}^2)^2 + \Gamma_{\mathcal{H}}^2 m_{\mathcal{H}}^2} \frac{\sum_i \Gamma(\tilde{\mathcal{H}} \rightarrow X_i)}{2m_S}, \quad (18)$$

$$\sigma_{ann} v_{rel}(F) = \frac{\lambda_{F\mathcal{H}}^2 m_F^2}{(4m_F^2 - m_{\mathcal{H}}^2)^2 + \Gamma_{\mathcal{H}}^2 m_{\mathcal{H}}^2} \frac{\sum_i \Gamma(\tilde{\mathcal{H}} \rightarrow X_i)}{2m_F} v_{rel}^2, \quad (19)$$

$$\sigma_{ann} v_{rel}(V) = \frac{2\lambda_{V\mathcal{H}}^2 v_0^2/3}{(4m_V^2 - m_{\mathcal{H}}^2)^2 + \Gamma_{\mathcal{H}}^2 m_{\mathcal{H}}^2} \frac{\sum_i \Gamma(\tilde{\mathcal{H}} \rightarrow X_i)}{2m_V}, \quad (20)$$

where  $v_{rel} = 2|p_D^{cm}|/m_D$  is the relative speed of the DM pair in their center-of-mass frame,  $\tilde{\mathcal{H}}$  is a virtual Higgs boson with the same couplings to other particles as the physical  $\mathcal{H}$  of mass  $m_{\mathcal{H}}$ , but with an invariant mass  $\sqrt{s} = 2m_D$ , and  $\tilde{\mathcal{H}} \rightarrow X_i$  is any possible decay mode of  $\mathcal{H}$  except that into dark matter.

As the non-SM Higgs does not couple to gauge bosons, it can only decay into fermion pairs and loop processes induced by Yukawa couplings besides DM singlet. In the Type II THDM, the Yukawa lagrangian is given by

$$\mathcal{L}_Y = -Y_2^u \bar{Q}_L \tilde{H}_2 U_R - Y_1^d \bar{Q}_L H_1 D_R - Y_1^l \bar{L}_L H_1 E_R + h.c. \quad (21)$$

where  $U_R$  is also an odd field under  $Z_2'$  symmetry. It leads to the following Yukawa interactions

$$\begin{aligned} \mathcal{L}_{ff\mathcal{H}} = & -\bar{U}_L M^u U_R \left( \frac{\cos \alpha}{\sin \beta} \frac{h^0}{v_0} + \frac{\sin \alpha}{\sin \beta} \frac{H^0}{v_0} \right) - \bar{D}_L M^d D_R \left( -\frac{\sin \alpha}{\cos \beta} \frac{h^0}{v_0} + \frac{\cos \alpha}{\cos \beta} \frac{H^0}{v_0} \right) \\ & - \bar{E}_L M^l E_R \left( -\frac{\sin \alpha}{\cos \beta} \frac{h^0}{v_0} + \frac{\cos \alpha}{\cos \beta} \frac{H^0}{v_0} \right) + h.c.. \end{aligned} \quad (22)$$

These Yukawa couplings also determine the singlet DM-nucleon scattering process with non-SM Higgs mediation in t-channel. Following Eq. (22), the non-SM Higgs  $\mathcal{H}$ - $q$ - $\bar{q}$  interactions  $\kappa_q^{\mathcal{H}}$  read

$$\kappa_u^H = \kappa_c^H = \kappa_t^H = \frac{\sin \alpha}{\sin \beta}, \quad \kappa_d^H = \kappa_s^H = \kappa_b^H = \frac{\cos \alpha}{\cos \beta}, \quad \text{for scenario I,} \quad (23)$$

$$\kappa_u^h = \kappa_c^h = \kappa_t^h = \frac{\cos \alpha}{\sin \beta}, \quad \kappa_d^h = \kappa_s^h = \kappa_b^h = -\frac{\sin \alpha}{\cos \beta}, \quad \text{for scenario II.} \quad (24)$$

It turns out that such THDM Yukawa couplings in the two limits are simplified into those in the MSSM

$$\frac{\sin \alpha}{\sin \beta} = \mp \frac{1}{\tan \beta}, \quad \frac{\cos \alpha}{\cos \beta} = \pm \tan \beta, \quad \tan \alpha = \frac{-1}{\tan \beta}, \quad \text{for } \sin(\beta - \alpha) = \pm 1 \text{ in scenario I,} \quad (25)$$

$$\frac{\cos \alpha}{\sin \beta} = \frac{1}{\tan \beta}, \quad -\frac{\sin \alpha}{\cos \beta} = -\tan \beta, \quad \tan \alpha = \tan \beta, \quad \text{for } \sin(\beta - \alpha) = 0 \text{ in scenario II.} \quad (26)$$

From Eqs. (25) and (26), one can see that the  $\mathcal{H}$ - $q$ - $\bar{q}$  interactions are independent of the choice of Higgs scenarios.

Combining the interactions of  $\mathcal{H}$ - $D$ - $D$  and  $\mathcal{H}$ - $q$ - $\bar{q}$ , the elastic cross sections of singlet DM with proton can be written as

$$\sigma_{el}^p(S) = \frac{\lambda_{S\mathcal{H}}^2 m_p^2 g_{pp\mathcal{H}}^2 v_0^2}{4\pi m_{\mathcal{H}}^4 (m_S + m_p)^2} = \frac{4m_p^2 m_S^2 f_{Sp}^2}{\pi (m_S + m_p)^2}, \quad f_{Sp} = \frac{\lambda_{S\mathcal{H}} g_{pp\mathcal{H}} v_0}{4m_S m_{\mathcal{H}}^2}, \quad (27)$$

$$\sigma_{el}^p(F) = \frac{\lambda_{F\mathcal{H}}^2 m_p^2 m_F^2 g_{pp\mathcal{H}}^2}{\pi m_{\mathcal{H}}^4 (m_F + m_p)^2} = \frac{4m_p^2 m_F^2 f_{Fp}^2}{\pi (m_F + m_p)^2}, \quad f_{Fp} = \frac{\lambda_{F\mathcal{H}} g_{pp\mathcal{H}}}{2m_{\mathcal{H}}^2}, \quad (28)$$

$$\sigma_{el}^p(V) = \frac{\lambda_{V\mathcal{H}}^2 m_p^2 g_{pp\mathcal{H}}^2 v_0^2}{4\pi m_{\mathcal{H}}^4 (m_V + m_p)^2} = \frac{4m_p^2 m_V^2 f_{Vp}^2}{\pi (m_V + m_p)^2}, \quad f_{Vp} = \frac{\lambda_{V\mathcal{H}} g_{pp\mathcal{H}} v_0}{4m_V m_{\mathcal{H}}^2}, \quad (29)$$

where  $g_{pp\mathcal{H}} = \sum_{u,d,s,c,b,t} g_q^p \kappa_q^{\mathcal{H}}$  and  $m_p$  denotes the mass of proton. If isospin-violating effect is taken into account, one has relation  $f_{Dn}/f_{Dp} = g_{nn\mathcal{H}}/g_{pp\mathcal{H}}$ . The relevant variables in Eqs. (27), (28) and (29) are collected in Appendix A for both isospin-conserving (IC) and isospin-violating (IV) cases.

### III. NUMERICAL RESULTS

For a given interaction between the WIMP and SM particles, the relic density  $\Omega_D$  can be calculated by [16]

$$\Omega_D h^2 \simeq \frac{1.07 \times 10^9 x_f}{M_{Pl} \sqrt{g_*} (a + 3b/x_f) \text{GeV}}, \quad x_f \simeq \ln \frac{0.038 M_{Pl} m_D (a + 6b/x_f)}{\sqrt{g_*} x_f}, \quad (30)$$

where  $a$  and  $b$  are the coefficients of the Taylor expansion in  $v_{rel}^2$  from the annihilation cross section  $\sigma_{ann} v_{rel} = a + b v_{rel}^2$ . Here  $h$  is the Hubble constant in the unit of  $100 \text{ km}/(s \cdot \text{Mpc})$ ,  $M_{Pl}$  is the Plank scale,  $x_f = m_D/T_f$  with  $T_f$  being the freezing temperature, and  $g_*$  is the total number of relativistic degrees of freedom at  $T_f$ . In Fig. 1 we show the restricted regions of  $x_f$  and  $\sigma_{ann} v_{rel}$  for pure S- and P-wave annihilation as a function of the WIMP mass  $m_D$ . They are obtained from Eq. (30) with  $\Omega_D h^2 = 0.1187 \pm 0.0017$  [17] and thus independent of the explicit form of the SM-WIMP interaction as well as other properties of the dark matter candidate. The freeze-out temperatures in both cases are almost the same with the one in S-wave slightly higher. The coefficient  $b$  in P-wave annihilation is nearly one order of magnitude larger than  $a$  in the S-wave case, as a result of compensating for the P-wave suppression.

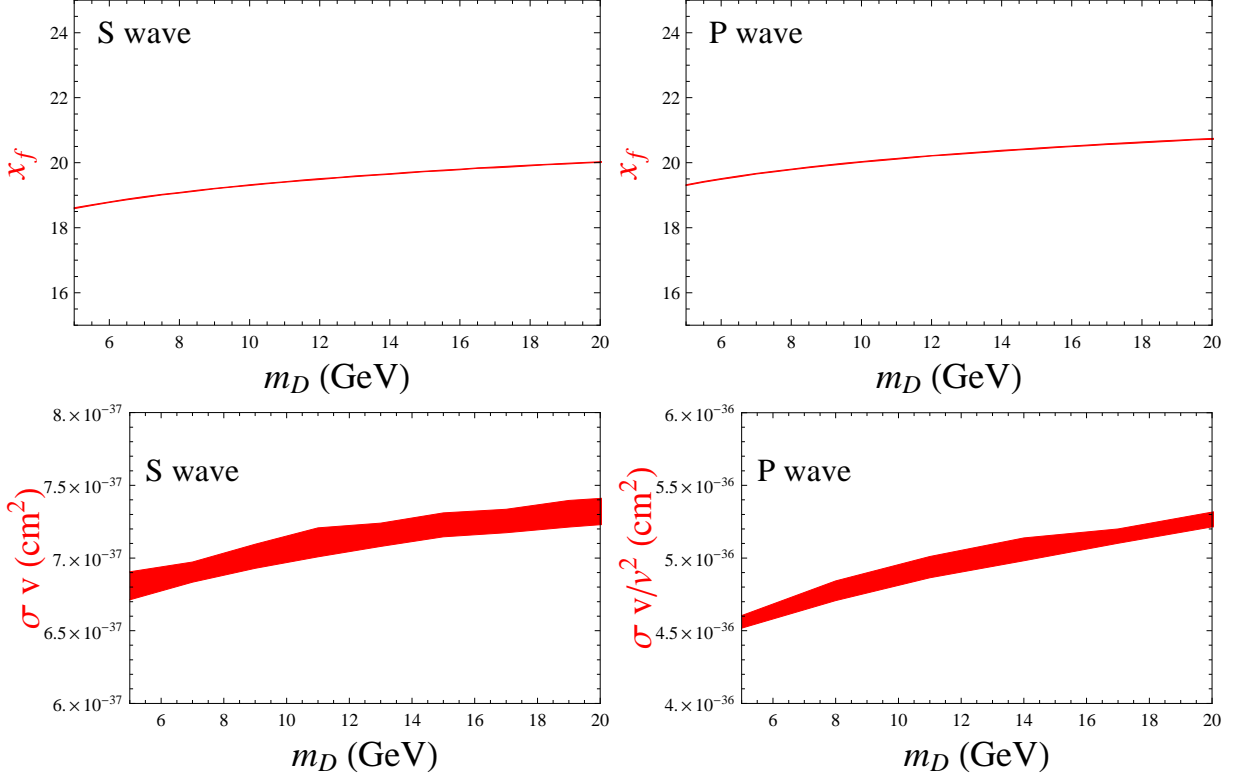


FIG. 1:  $x_f$  and  $\sigma_{ann}v_{rel}$  vs.  $m_D$  for annihilation in pure S- and P- waves.

#### A. Higgs-proton coupling $g_{pp\mathcal{H}}$ in both IC and IV cases

Due to the uncertainties of quark masses and hadronic matrix elements, the coupling  $g_{pp\mathcal{H}}$  may vary quite a bit. The dependence of  $g_{pp\mathcal{H}}$  on different hadronic quantities is shown in Appendix A. It is also determined by the Higgs-quark interactions  $\kappa_q^{\mathcal{H}}$ , namely  $\tan\beta$ , as shown in Eqs. (23) and (24). Thus, its absolute value is independent of different spectrum limits in Higgs sector. In Fig. 2 we show the coupling  $g_{pp\mathcal{H}}$  as a function of  $\tan\beta$  in both IC (top) and IV (bottom) cases. One can see that, in the IV case with  $f_{Dn}/f_{Dp} = -0.64$ , the coupling  $g_{pp\mathcal{H}}$  is nearly two orders of magnitude smaller compared to the one in IC case because of the medium  $\tan\beta$  values.

#### B. $\mathcal{H}$ - $D$ - $D$ coupling $\lambda_{D\mathcal{H}}$

The  $\mathcal{H}$ - $D$ - $D$  coupling  $\lambda_{D\mathcal{H}}$  can be derived from Eqs. (18), (19) and (20) for the scalar, fermion and vector DM, respectively. They should satisfy the restricted region of  $\sigma_{ann}v_{rel}$  shown in Fig. 1. In Fig. 3 we show the  $\lambda_{D\mathcal{H}}$  as a function of  $m_D$  for  $\tan\beta = 0.5$  and  $\tan\beta = 4.0$  with different

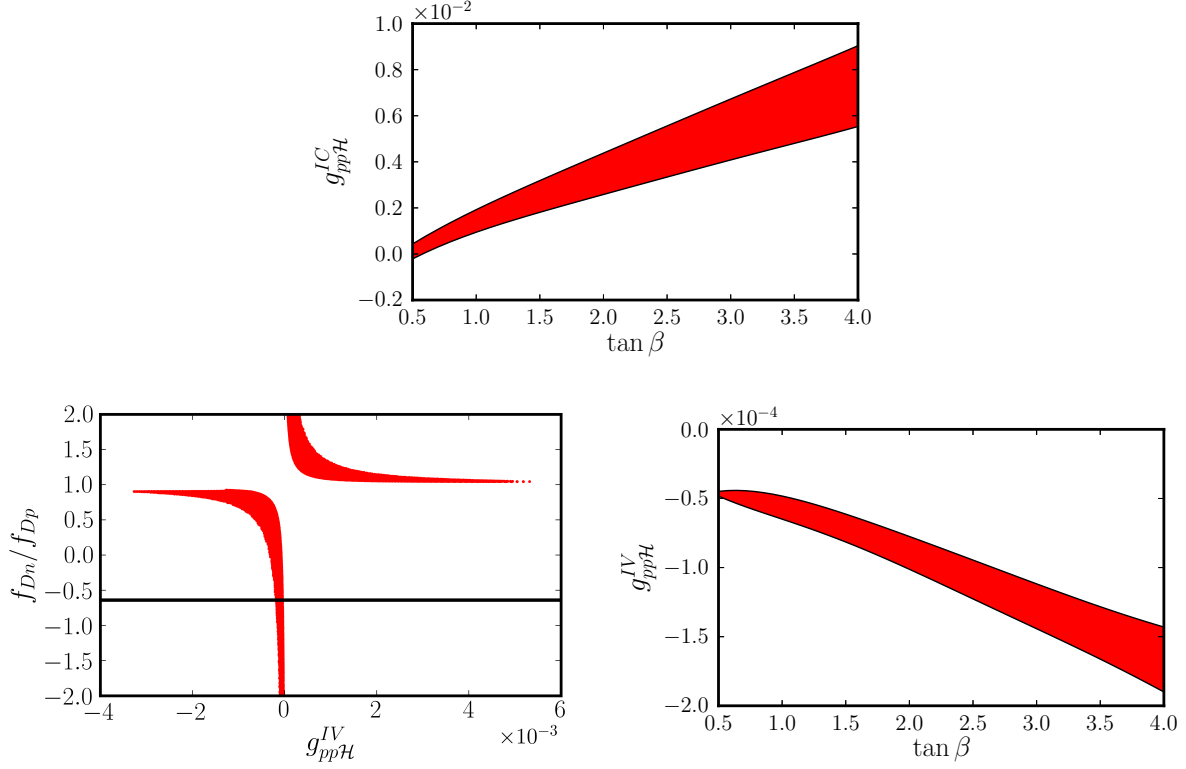


FIG. 2: Top:  $g_{pp\mathcal{H}}$  vs.  $\tan \beta$  for IC case ( $f_{Dn}/f_{Dp} = 1$ ). Bottom left: the scatter plot of  $f_{Dn}/f_{Dp}$  vs.  $g_{pp\mathcal{H}}$  for IV case ( $f_{Dn}/f_{Dp} \neq 1$ ) with  $0.5 < \tan \beta < 4$ . The horizontal line denotes the nearly xenon-phobic value  $f_{Dn}/f_{Dp} = -0.64$ . Bottom right:  $g_{pp\mathcal{H}}$  vs.  $\tan \beta$  for the xenon-phobic value,  $f_{Dn}/f_{Dp} = -0.64$ . These values of  $g_{pp\mathcal{H}}$  are for  $\sin(\beta - \alpha) = -1$  or  $0$ . The sign of the coupling should be flipped for  $\sin(\beta - \alpha) = 1$  case.

Higgs masses in the case of different dark matter spins. They produce the correct central value of dark matter relic abundance.

The scalar coupling  $\lambda_{S\mathcal{H}}$  is displayed in the top panel of Fig. 3. From Eq. (18), we know the scalar DM annihilation cross section approximately scales as

$$\sigma_{ann} v_{rel}(S) \sim \frac{3\lambda_{S\mathcal{H}}^2 m_b^2 \tan^2 \beta}{4\pi m_{\mathcal{H}}^4} \quad (31)$$

because the total decay width of Higgs is negligible compared with the Higgs mass in this case. Thus the coupling  $\lambda_{S\mathcal{H}}$  is almost independent of the dark matter mass when Higgs mass is relatively large. With the same Higgs mass but different  $\tan \beta$ , the only factor that changes in the annihilation cross section is  $\Gamma(\tilde{\mathcal{H}} \rightarrow X_i)$  which is dominated by  $\tilde{\mathcal{H}} \rightarrow b\bar{b}$ . Because the partial decay width of  $\mathcal{H} \rightarrow b\bar{b}$  is proportional to  $\tan^2 \beta$ , the smaller  $\lambda_{S\mathcal{H}}$  is required to achieve the cor-



rect annihilation cross section for larger  $\tan \beta$ . On the other hand, the annihilation cross section is always suppressed by the Higgs mass. For the same  $\tan \beta$ , therefore, the coupling  $\lambda_{S\mathcal{H}}$  should be smaller with decreasing Higgs mass.

For the fermionic dark matter, the dark matter annihilation is always P-wave suppressed. Thus the annihilation cross section is about one order of magnitude larger than the S-wave case, which in turn requires a large  $\lambda_{F\mathcal{H}}$ . Such a large  $\lambda_{F\mathcal{H}}$  leads to a large Higgs decay total width dominated by the invisible mode. The annihilation cross section is thus

$$\sigma_{ann} v_{rel}(F)/v_{rel}^2 \sim \frac{3\lambda_{F\mathcal{H}}^2 m_F^2 m_b^2 \tan^2 \beta / (8\pi v_0^2)}{m_{\mathcal{H}}^4 + m_{\mathcal{H}}^4 \lambda_{F\mathcal{H}}^4 / (16\pi)^2}. \quad (32)$$

The annihilation cross section in the fermionic dark matter case also has similar features with respect to DM mass,  $\tan \beta$  and  $m_{\mathcal{H}}$  as the scalar case. More importantly, at certain  $\lambda_{F\mathcal{H}}$  and with some small  $m_F$ , small  $\tan \beta$  and large  $m_{\mathcal{H}}$ , it reaches some value which does not necessarily fall into the restricted region as shown in bottom left panel of Fig. 3. We find that the annihilation cross section of fermion singlet DM into SM particles with any non-SM Higgs mass larger than 135 GeV would be too small. As a result, the fermion singlet does not apply for the degenerate case with heavy  $H^0$  in scenario I of THDM.

As seen from Eq. (17), the invisible decay of vector singlet DM is hugely enhanced by  $m_{\mathcal{H}}^3/m_V^4$ . Its annihilation cross section is thus approximately

$$\sigma_{ann} v_{rel}(V) \sim \frac{2\lambda_{V\mathcal{H}}^2 m_b^2 \tan^2 \beta / (8\pi)}{m_{\mathcal{H}}^4 + m_{\mathcal{H}}^8 \lambda_{V\mathcal{H}}^4 v_0^4 / (128\pi m_V^4)^2}. \quad (33)$$

Since this is pure S-wave annihilation, the coupling constant  $\lambda_{V\mathcal{H}}$  stays as large as in the scalar case. The scaling behavior of the annihilation cross section with respect to  $\lambda_{V\mathcal{H}}$ , however, is similar to the fermionic DM case because of the large invisible decay width. This feature also leads to the discontinued curves shown in the bottom right panel of Fig. 3. The reachable limit of non-SM Higgs mass in this case is also about 135 GeV.

### C. Coupling strength of the $D$ -proton elastic scattering: $f_{Dp}$

Combining the coupling  $g_{pp\mathcal{H}}$  and  $\lambda_{D\mathcal{H}}$  solved in previous subsections, we now proceed to study the elastic cross section of the singlet DM interacting with proton. The elastic cross section is determined by  $f_{Dp}$  as a product of  $g_{pp\mathcal{H}}$  and  $\lambda_{D\mathcal{H}}$  as shown in Eqs. (27), (28) and (29). In Fig. 4, we display  $f_{Dp}$  vs.  $m_D$  for different  $\tan \beta$  with and without isospin violation. From Fig. 2

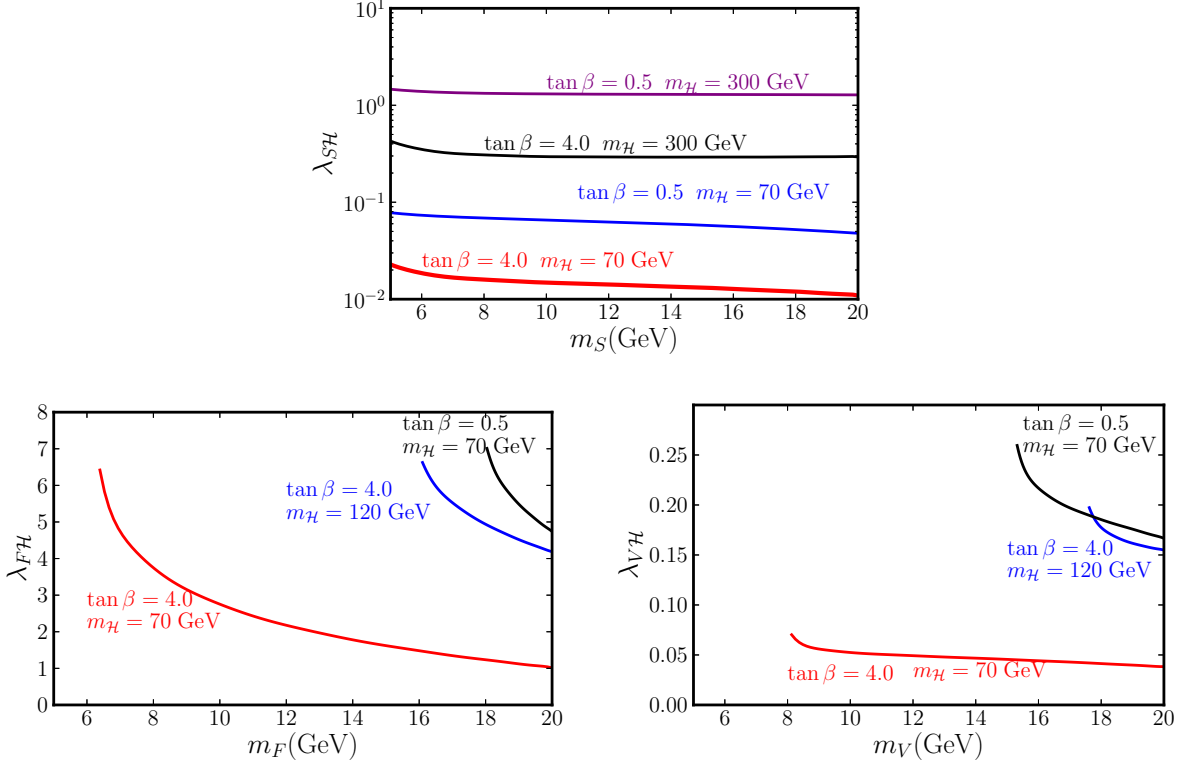


FIG. 3: Top:  $\lambda_{S\mathcal{H}}$  vs.  $m_S$  for  $\tan\beta = 0.5$  and  $\tan\beta = 4.0$  with  $m_{\mathcal{H}} = 70$  GeV and  $m_{\mathcal{H}} = 300$  GeV. Bottom:  $\lambda_{F\mathcal{H}}$  vs.  $m_F$  (left) and  $\lambda_{V\mathcal{H}}$  vs.  $m_V$  (right) for  $\tan\beta = 0.5$  and  $\tan\beta = 4.0$  with  $m_{\mathcal{H}} = 70$  GeV and  $m_{\mathcal{H}} = 120$  GeV.

and Fig. 3, we see that the  $\lambda_{D\mathcal{H}}$  decreases with increasing  $\tan\beta$  while the absolute value of  $g_{pp\mathcal{H}}$  increases in both IC and IV cases. In particular,  $g_{pp\mathcal{H}}$  in the IC case increases more quickly than the decreasing of the  $\lambda_{D\mathcal{H}}$  with increasing  $\tan\beta$ , which results in an increasing  $f_{Dp}$  with increasing  $\tan\beta$ . In the IV case, however, the increasing of  $g_{pp\mathcal{H}}$  is slower and it leads to an opposite trend with  $\tan\beta$  for all DM singlets. The overall scale of  $f_{Dp}$  in the IV case is much smaller than IC case since the coupling  $g_{pp\mathcal{H}}$  in the IV case is two orders of magnitude smaller. Moreover,  $f_{Sp}$  for different masses of Higgs remains the same as the Higgs mass dependence is cancelled in Eq. (27). We thus show  $f_{Dp}$  for only one particular Higgs mass in Fig. 4

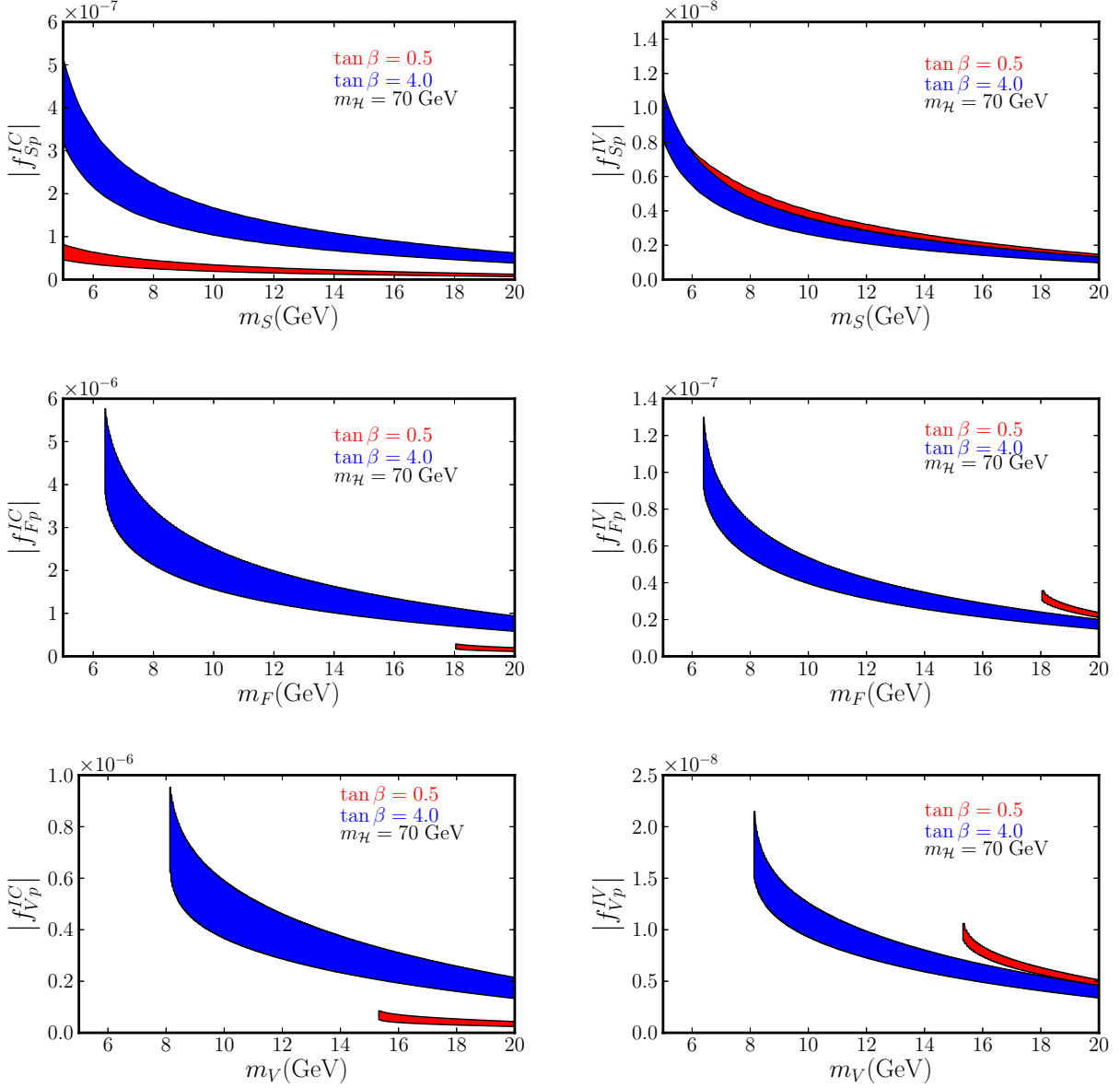


FIG. 4: Top:  $f_{Sp}$  vs.  $m_S$  for  $\tan \beta = 0.5$  and  $\tan \beta = 4.0$  with  $m_{\mathcal{H}} = 70$  GeV. Middle:  $f_{Fp}$  vs.  $m_F$  for  $\tan \beta = 0.5$  and  $\tan \beta = 4.0$  with  $m_{\mathcal{H}} = 70$  GeV. Bottom:  $f_{Vp}$  vs.  $m_V$  for  $\tan \beta = 0.5$  and  $\tan \beta = 4.0$  with  $m_{\mathcal{H}} = 70$  GeV. Left column: IC case with  $f_{Dn}/f_{Dp} = 1$ ; Right column: IV case with  $f_{Dn}/f_{Dp} = -0.64$ .

#### D. Invisible decay of singlet DM

Now we turn to the decay branching ratio of the Higgs  $\mathcal{H}$ , as shown in Fig. 5 for different Higgs mass,  $\tan \beta$  and singlet DM candidates. The branching ratios here are calculated with the

coupling  $\lambda_{D\mathcal{H}}$  from Fig. 3. The common feature is that the Higgs decay width is significantly dominated by the invisible channel  $\mathcal{H} \rightarrow DD$ . The other major contribution comes from  $\mathcal{H} \rightarrow b\bar{b}$  and  $\mathcal{H} \rightarrow \tau^+\tau^-$ . Such significant invisible decay in THDM can be tested through mono-b jet process  $gb \rightarrow b\mathcal{H}$ .

#### E. $D$ -proton elastic scattering cross section $\sigma_{el}^p$

At last we gather all the necessary ingredients to calculate the elastic cross section of dark matter scattering with proton according to Eqs. (27), (28) and (29). The uncertainties come from the measurement of the dark matter relic abundance  $\Omega h^2$  and the coupling  $g_{pp\mathcal{H}}$ . The results for IC and IV case with various singlet DM candidates and  $m_{\mathcal{H}} = 70$  GeV are shown in Fig. 6. For scalar singlet, the lower (upper) and upper (lower) limit of the elastic cross section is obtained with  $\tan\beta = 0.5$  and  $\tan\beta = 4.0$  in the IC (IV) case. As stated before, these limits apply for any values of  $m_{\mathcal{H}}$  in this case. Fig. 6a shows that the restricted region of the parameter space is consistent with most of the region of interests (ROI) of CDMS-Si for scalar DM with IC, while the IV case (Fig. 6b) has a two orders of magnitude smaller elastic cross section due to the much small  $g_{pp\mathcal{H}}$ .

For fermionic singlet DM (see Figs. 6c and 6d), the elastic cross section in the restricted region is about two orders of magnitude larger than the scalar case, since the annihilation cross section is P-wave suppressed and a much larger  $\mathcal{H}$ - $D$ - $D$  coupling is needed. Similar to the scalar DM, the fermion elastic cross section increase with increasing  $\tan\beta$  in the IC case and decreases in the IV case. For larger  $m_{\mathcal{H}}$ , the allowed region of elastic cross section is more restricted and only covers relatively large values of  $m_F$ .

In the vector DM case (see Figs. 6e and 6f), the elastic cross section is of the same order of magnitude as the scalar DM case. But the restricted region is narrower and overlaps much less with the ROIs of CDMS-Si than the scalar DM case. It is because the enhanced dark matter decay width suppresses the total annihilation cross section in some parameter space and the restricted region is further constrained as already explained in Sec. III B.

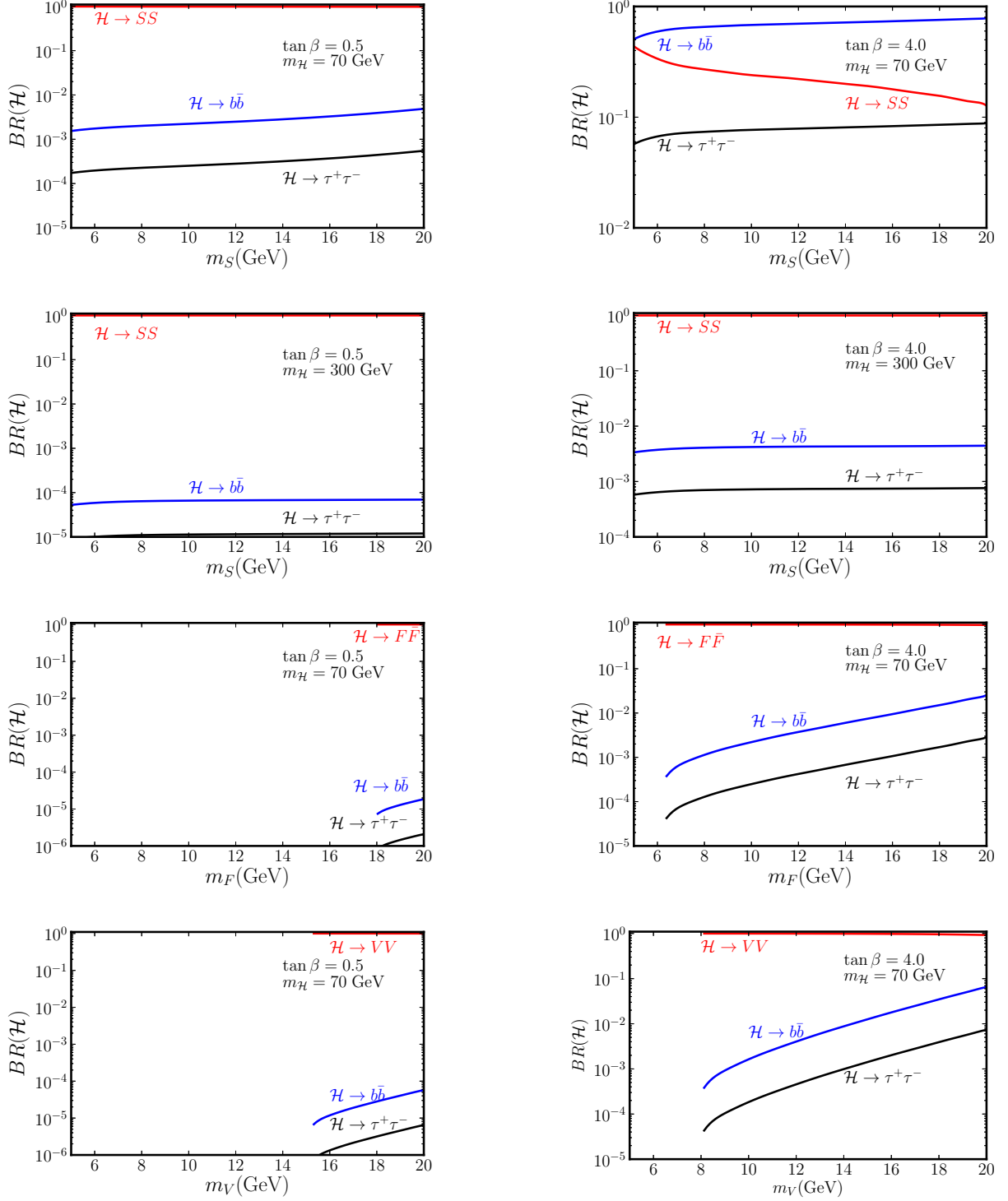


FIG. 5:  $BR(\mathcal{H})$  vs.  $m_S$  with  $\tan\beta = 0.5$  and  $\tan\beta = 4$  for  $m_{\mathcal{H}} = 70$  GeV (1st row) and 300 GeV (2nd row).  $BR(\mathcal{H})$  vs.  $m_F$  with  $\tan\beta = 0.5$  and  $\tan\beta = 4$  for  $m_{\mathcal{H}} = 70$  GeV (3rd row) and the same parameters for the vector case (4th row).

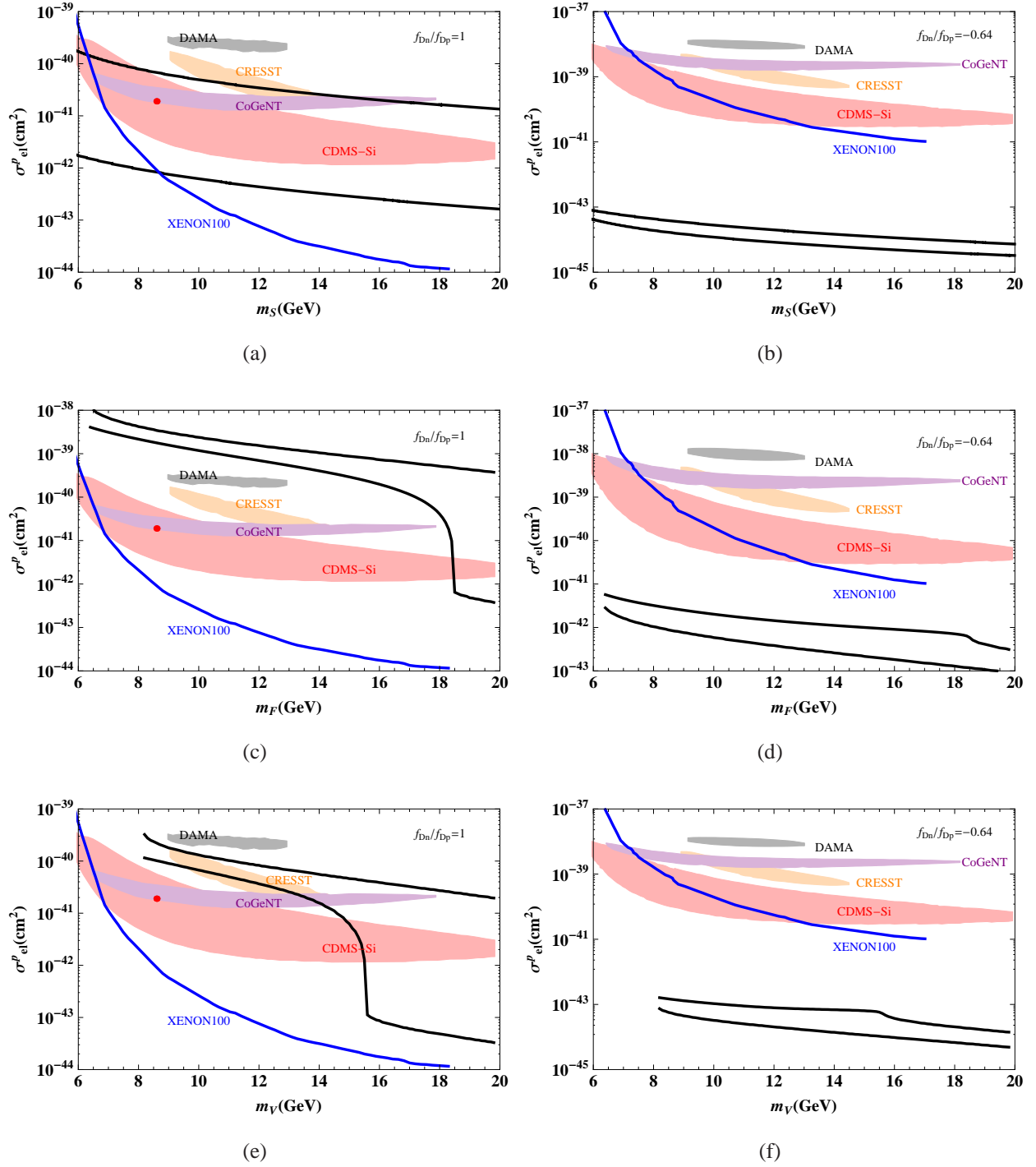


FIG. 6: Top: The elastic cross section of scalar DM with proton. Middle: The elastic cross section of fermionic DM with proton. Bottom: The elastic cross section of vector DM with proton. Left column: IC case with  $f_{Dn}/f_{Dp} = 1$ ; Right column: IV case with  $f_{Dn}/f_{Dp} = -0.64$ .

$m_{\mathcal{H}}$  is fixed to be 70 GeV and  $\tan \beta$  varies from 0.5 to 4. The 90% CL ROIs for CDMS-Si, CoGeNT, and the  $3(2)\sigma$  ROIs for DAMA (CRESST-II) are also plotted together with the exclusion limits from XENON100. The red point denotes the best fitted result from CDMS-Si.

## IV. CONCLUSIONS

The light WIMP dark matter is of special interests given the recent events from direct detection experiments. We have studied the simple extension of the minimal SM with two Higgs doublets and a SM gauge singlet stabilized by  $Z_2$  symmetry in the low mass region. We focused on the Type II THDM with a vanishing coupling between the singlet dark matter and the SM-like Higgs such that single DM can only couple to the non-SM Higgs in pairs. The SM-like Higgs invisible decay is thus consistent with LHC search. In this limit, the only parameters of the model include the dark matter mass  $m_D$ , the non-SM CP-even Higgs mass  $m_{\mathcal{H}}$ ,  $\tan \beta$  and the  $\mathcal{H} - D - D$  coupling  $\lambda_{D\mathcal{H}}$ .

To obtain appropriate dark matter relic abundance, we found in the case of fermionic singlet, a large coupling  $\lambda_{F\mathcal{H}}$  is required because of P-wave suppression. In the vector singlet case, the coupling  $\lambda_{V\mathcal{H}}$  remains at the same order as that of the scalar case, but one order of magnitude smaller than the fermion case. The Higgs decay width is dominated by the invisible mode. In both fermionic and vector DM case the large invisible decay width leads to a suppressed annihilation cross section. In some parameter space, the dark matter would overclose the universe.

We also considered the hadronic uncertainties in both isospin conserving and isospin violating cases (especially the nearly xenon-phobic case with  $f_{Dn}/f_{Dp} = -0.64$ ). It turns out in this model, with LHC favored parameter region, the Higgs-proton coupling  $g_{pp\mathcal{H}}$  in the IV case is almost two orders of magnitude smaller than that in IC case. This feature would definitely suppress the elastic scattering cross section between dark matter and nucleon.

After scanning the allowed parameter space, we found that only the scalar singlet without IV effects has a major overlap with the region of interests of most direct detection experiments although it is still in tension with XENON100. The elastic cross section in the IC fermionic case is much larger than all the experimental ROIs due to the large coupling  $\lambda_{F\mathcal{H}}$  which is required to compensate for the P-wave suppression. The vector case has less overlap with the experimental ROIs because in some parameter space the large invisible decay width leads to an overclosed universe. All the scenarios in the IV case have small elastic cross section because of the small Higgs-proton coupling.

## Acknowledgment

We would like to thank Robert Foot, Michael A. Schmidt, Shufang Su and Felix Yu for useful discussions. T.L. would also like to thank Fermilab for the hospitality during which part of this work was carried out. This work was supported in part by the Australian Research Council.

## Appendix A: Higgs-nucleon couplings

For isospin-conserving case ( $f_{Dn}/f_{Dp} = 1$ ), the  $g_q^N$ s ( $N = n, p$ ) are [10, 18]

$$g_u^N = g_d^N = \frac{\sigma_{\pi N}}{2v_0}, \quad g_s^N = \frac{m_N - m_B - \sigma_{\pi N}}{v_0}, \quad g_Q^N = \frac{2m_B}{27v_0}, \quad (\text{A1})$$

$$m_B = -\sigma_{\pi N} \frac{2m_K^2 + m_\pi^2}{2m_\pi^2} + \frac{(m_\Xi + m_\Sigma)(2m_K^2 - m_\pi^2) - 2m_N m_\pi^2}{4(m_K^2 - m_\pi^2)}. \quad (\text{A2})$$

For isospin-violating case ( $f_{Dn}/f_{Dp} \neq 1$ ), they are [11, 18–21]

$$g_q^N = \frac{B_q^N m_q}{v_0}, \quad q = u, d, s; \quad g_Q^N = \frac{2}{27v_0} \left( m_N - \sum_q m_q B_q^N \right), \quad Q = c, b, t, \quad (\text{A3})$$

$$B_u^N = \frac{2\sigma_{\pi N}}{m_u(1 + \frac{m_d}{m_u})(1 + \frac{B_d^N}{B_u^N})}, \quad B_d^N = \frac{2\sigma_{\pi N}}{m_d(1 + \frac{m_u}{m_d})(1 + \frac{B_u^N}{B_d^N})}, \quad B_s^N = \frac{\frac{m_s}{m_d}\sigma_{\pi N}(1 - \frac{\sigma_0}{\sigma_{\pi N}})}{m_s(1 + \frac{m_u}{m_d})}, \quad (\text{A4})$$

$$\frac{B_d^p}{B_u^p} = \frac{2 + (z - 1)(1 - \frac{\sigma_0}{\sigma_{\pi N}})}{2z - (z - 1)(1 - \frac{\sigma_0}{\sigma_{\pi N}})}, \quad B_u^n = B_d^p, \quad B_d^n = B_u^p, \quad (\text{A5})$$

$$\frac{m_u}{m_d} = 0.38 - 0.58, \quad \frac{m_s}{m_d} = 17 - 22, \quad z \equiv \frac{B_u^p - B_s^p}{B_d^p - B_s^p} = 1.49, \quad (\text{A6})$$

$$\sigma_0 = 58 \pm 9 \text{ MeV}, \quad \sigma_{\pi N} = 58 \pm 9 \text{ MeV}. \quad (\text{A7})$$

- 
- [1] R. Bernabei *et al.* [DAMA and LIBRA Collaborations], *Eur. Phys. J. C* **67**, 39 (2010) [arXiv:1002.1028 [astro-ph.GA]].
  - [2] C. E. Aalseth *et al.* [CoGeNT Collaboration], *Phys. Rev. Lett.* **106**, 131301 (2011) [arXiv:1002.4703 [astro-ph.CO]].
  - [3] G. Angloher, M. Bauer, I. Bavykina, A. Bento, C. Bucci, C. Ciemniak, G. Deuter and F. von Feilitzsch *et al.*, *Eur. Phys. J. C* **72**, 1971 (2012) [arXiv:1109.0702 [astro-ph.CO]].
  - [4] R. Agnese *et al.* [CDMS Collaboration], [arXiv:1304.4279 [hep-ex]].
  - [5] V. Silveira and A. Zee, *Phys. Lett. B* **161**, 136 (1985).



- [6] C. P. Burgess, M. Pospelov and T. ter Veldhuis, Nucl. Phys. B **619**, 709 (2001) [hep-ph/0011335].
- [7] J. McDonald, Phys. Rev. D **50**, 3637 (1994) [hep-ph/0702143 [HEP-PH]].
- [8] M.C. Bento, O. Bertolami, R. Rosenfeld, and L. Teodoro, *ibid.* **62**, 041302 (2000) [arXiv:astro-ph/0003350]; D.E. Holz and A. Zee, Phys. Lett. B **517**, 239 (2001) [arXiv:hep-ph/0105284]. M.C. Bento, O. Bertolami, and R. Rosenfeld, *ibid.* **518**, 276 (2001) [arXiv:hep-ph/0103340]; J. McDonald, Phys. Rev. Lett. **88**, 091304 (2002) [arXiv:hep-ph/0106249]; C. Bird, P. Jackson, R. Kowalewski, and M. Pospelov, *ibid.* **93**, 201803 (2004) [arXiv:hep-ph/0401195]; H. Davoudiasl, R. Kitano, T. Li, and H. Murayama, Phys. Lett. B **609**, 117 (2005) [arXiv:hep-ph/0405097]. G. Cynolter, E. Lendvai, and G. Pocsik, Acta Phys. Polon. B **36**, 827 (2005) [arXiv:hep-ph/0410102]; C. Bird, R. Kowalewski, and M. Pospelov, Mod. Phys. Lett. A **21**, 457 (2006) [arXiv:hep-ph/0601090]; S.h. Zhu, arXiv:hep-ph/0601224; S. Andreas, T. Hambye, and M.H.G. Tytgat, JCAP **0810**, 034 (2008) [arXiv:0808.0255 [hep-ph]]; W. -L. Guo and Y. -L. Wu, JHEP **1010**, 083 (2010) [arXiv:1006.2518 [hep-ph]]; V. Barger, Y. Gao, M. McCaskey and G. Shaughnessy, Phys. Rev. D **82**, 095011 (2010) [arXiv:1008.1796 [hep-ph]]; S. Profumo, L. Ubaldi and C. Wainwright, Phys. Rev. D **82**, 123514 (2010) [arXiv:1009.5377 [hep-ph]]; J. R. Espinosa, T. Konstandin and F. Riva, Nucl. Phys. B **854**, 592 (2012) [arXiv:1107.5441 [hep-ph]]; Y. Mambrini, Phys. Rev. D **84**, 115017 (2011) [arXiv:1108.0671 [hep-ph]]; I. Low, P. Schwaller, G. Shaughnessy and C. E. M. Wagner, Phys. Rev. D **85**, 015009 (2012) [arXiv:1110.4405 [hep-ph]]; A. Djouadi, O. Lebedev, Y. Mambrini and J. Quevillon, Phys. Lett. B **709**, 65 (2012) [arXiv:1112.3299 [hep-ph]]; K. Cheung, Y. -L. S. Tsai, P. -Y. Tseng, T. -C. Yuan and A. Zee, JCAP **1210**, 042 (2012) [arXiv:1207.4930 [hep-ph]].
- [9] X. -G. He, T. Li, X. -Q. Li and H. -C. Tsai, Mod. Phys. Lett. A **22**, 2121 (2007) [hep-ph/0701156]; X. -G. He, T. Li, X. -Q. Li, J. Tandean and H. -C. Tsai, Phys. Lett. B **688**, 332 (2010) [arXiv:0912.4722 [hep-ph]]; X. -G. He, S. -Y. Ho, J. Tandean and H. -C. Tsai, Phys. Rev. D **82**, 035016 (2010) [arXiv:1004.3464 [hep-ph]].
- [10] X. -G. He, T. Li, X. -Q. Li, J. Tandean and H. -C. Tsai, Phys. Rev. D **79**, 023521 (2009) [arXiv:0811.0658 [hep-ph]].
- [11] J. M. Cline, K. Kainulainen, P. Scott and C. Weniger, arXiv:1306.4710 [hep-ph].
- [12] Y. Cai, X. -G. He and B. Ren, Phys. Rev. D **83**, 083524 (2011) [arXiv:1102.1522 [hep-ph]]; T. Li and Q. Shafi, Phys. Rev. D **83**, 095017 (2011) [arXiv:1101.3576 [hep-ph]]; Y. Bai, V. Barger, L. L. Everett and G. Shaughnessy, Phys. Rev. D **88**, 015008 (2013) [arXiv:1212.5604 [hep-ph]]; X. -G. He and J. Tandean, Phys. Rev. D **88**, 013020 (2013) [arXiv:1304.6058 [hep-ph]].

- [13] J. L. Feng, J. Kumar and D. Sanford, Phys. Rev. D **88**, 015021 (2013) [arXiv:1306.2315 [hep-ph]].
- [14] B. nGrinstein and P. Uttayarat, JHEP **1306**, 094 (2013) [arXiv:1304.0028 [hep-ph]]; B. Coleppa, F. Kling and S. Su, arXiv:1305.0002 [hep-ph]; C. -Y. Chen, S. Dawson and M. Sher, Phys. Rev. D **88**, 015018 (2013) [arXiv:1305.1624 [hep-ph]]; O. Eberhardt, U. Nierste and M. Wiebusch, arXiv:1305.1649 [hep-ph]; V. Barger, L. L. Everett, H. E. Logan and G. Shaughnessy, arXiv:1308.0052 [hep-ph].
- [15] S. Kanemura, S. Matsumoto, T. Nabeshima and N. Okada, Phys. Rev. D **82**, 055026 (2010) [arXiv:1005.5651 [hep-ph]].
- [16] E. W. Kolb and M. Turner, The Early Universe (Westview Press, Boulder, 1990).
- [17] P. A. R. Ade *et al.* [Planck Collaboration], arXiv:1303.5062 [astro-ph.CO].
- [18] J. R. Ellis, K. A. Olive and C. Savage, Phys. Rev. D **77**, 065026 (2008) [arXiv:0801.3656 [hep-ph]].
- [19] J. Beringer *et al.* (Particle Data Group), Phys. Rev. D **86**, 010001 (2012).
- [20] J. M. Alarcon, J. Martin Camalich and J. A. Oller, Annals Phys. **336**, 413 (2013) [arXiv:1210.4450 [hep-ph]].
- [21] L. Alvarez-Ruso, T. Ledwig, J. Martin Camalich and M. J. Vicente-Vacas, arXiv:1304.0483 [hep-ph].